



## Technical note

## Musculoskeletal model-based inverse dynamic analysis under ambulatory conditions using inertial motion capture

Angelos Karatsidis<sup>a,b,\*</sup>, Moonki Jung<sup>c</sup>, H. Martin Schepers<sup>a</sup>, Giovanni Bellusci<sup>a</sup>, Mark de Zee<sup>d</sup>, Peter H. Veltink<sup>b</sup>, Michael Skipper Andersen<sup>e</sup>

<sup>a</sup>Xsens Technologies B.V., Pantheon 6-8, Enschede 7521 PR, the Netherlands

<sup>b</sup>Department of Biomedical Signals and Systems, Faculty of Electrical Engineering, Mathematics and Computer Science, Technical Medical Centre, University of Twente, Enschede 7500 AE, the Netherlands

<sup>c</sup>AnyBody Technology A/S, Aalborg 9220, Denmark

<sup>d</sup>Department of Health Science and Technology, Aalborg University, Aalborg 9220, Denmark

<sup>e</sup>Department of Materials and Production, Aalborg University, Aalborg 9220, Denmark



## ARTICLE INFO

## Article history:

Received 15 February 2018

Revised 26 September 2018

Accepted 16 December 2018

## Keywords:

Musculoskeletal modeling

Inertial motion capture

Inverse dynamics

Ground reaction forces and moments

Gait analysis

## ABSTRACT

Inverse dynamic analysis using musculoskeletal modeling is a powerful tool, which is utilized in a range of applications to estimate forces in ligaments, muscles, and joints, non-invasively. To date, the conventional input used in this analysis is derived from optical motion capture (OMC) and force plate (FP) systems, which restrict the application of musculoskeletal models to gait laboratories. To address this problem, we propose the use of inertial motion capture to perform musculoskeletal model-based inverse dynamics by utilizing a universally applicable ground reaction force and moment (GRF&M) prediction method. Validation against a conventional laboratory-based method showed excellent Pearson correlations for sagittal plane joint angles of ankle, knee, and hip ( $\rho = 0.95$ ,  $0.99$ , and  $0.99$ , respectively) and root-mean-squared-differences (RMSD) of  $4.1 \pm 1.3^\circ$ ,  $4.4 \pm 2.0^\circ$ , and  $5.7 \pm 2.1^\circ$ , respectively. The GRF&M predicted using IMC input were found to have excellent correlations for three components (vertical:  $\rho = 0.97$ ,  $\text{RMSD} = 9.3 \pm 3.0\% \text{BW}$ , anteroposterior:  $\rho = 0.91$ ,  $\text{RMSD} = 5.5 \pm 1.2\% \text{BW}$ , sagittal:  $\rho = 0.91$ ,  $\text{RMSD} = 1.6 \pm 0.6\% \text{BW} \cdot \text{BH}$ ), and strong correlations for mediolateral ( $\rho = 0.80$ ,  $\text{RMSD} = 2.1 \pm 0.6\% \text{BW}$ ) and transverse ( $\rho = 0.82$ ,  $\text{RMSD} = 0.2 \pm 0.1\% \text{BW} \cdot \text{BH}$ ). The proposed IMC-based method removes the complexity and space restrictions of OMC and FP systems and could enable applications of musculoskeletal models in either monitoring patients during their daily lives or in wider clinical practice.

© 2019 IPEM. Published by Elsevier Ltd. All rights reserved.

## 1. Introduction

Assessment of muscle, joint, and ligament forces is important to understand the mechanical and physiological mechanisms of human movement. To date, the measurement of such in-vivo forces is a challenging task. For this reason, computer-based musculoskeletal models have been widely used to estimate the variables of interest non-invasively [1,2].

The most common approach used in musculoskeletal modeling is the method of the inverse dynamics [3]. This analysis utilizes the equations of motion with input from human body kinematics in conjunction with kinetics obtained from external forces [4], to estimate joint reaction and muscle forces, as well as net joint

moments using muscle recruitment methods [5]. Measurements of the external forces are typically required and measured using force plates (FPs), however, the use of FPs has several limitations. First, subjects tend to alter their natural gait patterns in order to hit the small and fixed measurement area of a plate [6]. In addition, this static and limited measurement area, impedes the assessment of several consecutive steps, when only a couple of FPs are available. Finally, the combined use of FP with motion input introduces a dynamic inconsistency, which results to residual forces and moments in the inverse dynamics [7,8].

Several studies have proposed replacing the FP input with wearable devices such as shoes with three-dimensional force and torque sensors beneath the sole [9–11]. In a similar fashion, pressure insoles were proposed to reconstruct the complete ground reaction forces and moments (GRF&M) from pressure distributions [12–14]. Although these wearable devices are suitable for the assessment of external forces, the increased height and weight of the shoes equipped with force/torque sensors [15,16], as well as the

\* Corresponding author at: Xsens Technologies B.V., Pantheon 6-8, Enschede 7521 PR, the Netherlands.

E-mail address: [angelos.karatsidis@xsens.com](mailto:angelos.karatsidis@xsens.com) (A. Karatsidis).

repeatability of the pressure sensors [17] are considered important limitations.

Recent research has suggested the replacement of the force input with predictions derived solely from motion input [18–23]. In these studies, human body kinematics are combined with the inertial properties of the body segments, from which Newton–Euler equations are utilized to compute the external forces and moments. Since the system of equations becomes indeterminate during the double stance of gait, each of the aforementioned studies focused on methods to solve this issue. Ren et al. [19] suggested a gait event-based function which is only applicable in gait, while Oh et al. [20] and Choi et al. [21] suggested methods based on a machine learning that require a training database and thus are not applicable for movements not included in that database. A last approach enables the universal application of these methods using a muscle recruitment approach has shown promising performance for various activities of daily living [22] and sports [23].

The majority of the existing research which studied the prediction of GRF&M, used conventional optical motion capture (OMC) input. Despite the high accuracy of this method in tracking marker trajectories, its dependence on laboratory equipment restricts possible applications during daily life activities or in wider clinical practice. In the previous decade, ambulatory motion tracking systems based on inertial measurement units (IMUs), have been proposed as a suitable alternative for estimating 3D segment kinematics [24–27]. A key benefit of such systems is that they can be applied in virtually any environment without depending on external infrastructure, such as cameras. Driven by these advances in inertial motion capture (IMC), recent work of the authors demonstrated its ability to estimate three-dimensional GRF&M [28], which were distributed between the feet using a smooth transition assumption concept [19]. However, limitations of that approach is that it is only valid for gait and has no muscle, bone or ligament force estimate capabilities.

To date, the use of detailed musculoskeletal modeling with kinematic inputs from IMUs has only received limited attention. Koning et al. [29] previously demonstrated the feasibility of kinematically driving a musculoskeletal model using only orientations from IMUs. However, that study only compared the kinematics of the musculoskeletal model, without any inverse dynamic calculations.

The aim of this study was to develop a workflow to perform musculoskeletal model-based inverse dynamics using exclusively IMC input, applicable in ambulatory environments and validate it against a conventional laboratory-based approach.

## 2. Methods

### 2.1. Subjects

The experimental data was collected at the Human Performance Laboratory, at the Department of Health Science and Technology, Aalborg University, Aalborg, Denmark following the ethical guidelines of The Scientific Ethical Committee for the Region of North Jutland (Den Videnskabssetiske Komité for Region Nordjylland). Eleven healthy male individuals with no present musculoskeletal or neuromuscular disorders volunteered for the study (age:  $31.0 \pm 7.2$  years; height:  $1.81 \pm 0.06$  m; weight:  $77.3 \pm 9.2$  kg; body mass index (BMI):  $23.6 \pm 2.4$  kg/m<sup>2</sup>). All participants provided written informed consent, prior to data collection.

### 2.2. Instrumentation

Full-body IMC data were collected using the Xsens MVN Link (Xsens Technologies B.V., Enschede, the Netherlands), in which 17 IMUs were mounted on the head, sternum, pelvis, upper legs,

lower legs, feet, shoulders, upper arms, forearms and hands using the dedicated clothing. The exact location of each sensor on the respective segment followed the manufacturer guidelines described in the manual of Xsens MVN [30]. The affiliated software Xsens MVN Studio 4.2.4 was used to track the IMU orientations with respect to an earth-based coordinate frame [24,25]. Segment orientations were obtained by applying the IMU-to-segment alignment, found using a known upright pose (N-pose) performed by the subject at a known moment in time, while taking specific care to minimize the effect of magnetic disturbances. In addition, this information is fused with updates regarding the joints and external contacts to limit the position drift [26].

For validation purposes, an OMC system utilizing 8 infrared high speed cameras (Oqus 300 series, Qualisys AB, Gothenburg, Sweden) and the software Qualisys Track Manager 2.12 (QTM) were used to track the trajectories of 53 reflective markers mounted on the human body, as described in the Appendix of [28]. In addition, three FP systems (AMTI OR6-7-1000, Advanced Mechanical Technology, Inc., Watertown, MA, USA) embedded in the floor of the laboratory, were utilized using QTM to record the GRF&Ms. Both IMC and OMC systems sampled data at a frequency of 240 Hz, while the FP system sampled data at 2400 Hz and subsequently downsampled to 240 Hz to match the IMC and OMC sampling rate. A second-order forward-backward low-pass Butterworth filter was applied to the reflective marker trajectories and measured GRF&M, with cut-off frequencies of 6 Hz and 15 Hz, respectively.

### 2.3. Experimental protocol

For each participant, the body dimensions were extracted using a conventional tape following the guidelines of Xsens. During the data collection, the subjects were instructed to walk barefoot in three different walking speeds (comfortable; CW, fast; FW, and slow; SW). The walking speeds performed experimentally were quantified as  $1.28 \pm 0.14$  m/s (mean  $\pm$  standard deviation) for CW,  $1.58 \pm 0.09$  m/s for FW (CW + 23%) and  $0.86 \pm 0.11$  m/s for SW (CW – 33%). For every walking speed, five successful trials were assessed. A successful trial was obtained when a single foot hit one of the FPs entirely, followed by an entire hit of the other foot on the successive FP.

### 2.4. Overall description of the components in the musculoskeletal models

Three musculoskeletal models have been constructed in AnyBody™ Modeling System (AMS) v.6.0.7 (AnyBody™ Technology A/S, Aalborg, Denmark) [1]:

- a model in which the kinematics are driven by IMC and the GRF&M are predicted from the kinematics (IMC-PGRF).
- a model in which the kinematics are driven by OMC and the GRF&M are predicted from the kinematics (OMC-PGRF).
- a model in which the kinematics are driven by OMC and the GRF&M are measured from FPs (OMC-MGRF).

In the IMC-PGRF model, a Biovision Hierarchy (BVH) file is exported from Xsens MVN Studio and imported in AMS, in which a stick figure model is initially reconstructed. The BVH file contains a hierarchy part with a description of the linked segment model in a static pose, as well as a motion part that contains, for each time frame, the absolute position and orientation of the root pelvis segment, and the joint angles between the segments described in the hierarchy. The generated stick figure model contains 72 degrees-of-freedom (DOF). In order to match the stick figure model with the musculoskeletal model, we utilize a concept of virtual markers (VMs) demonstrated in a previous Kinect-based study [31]. The

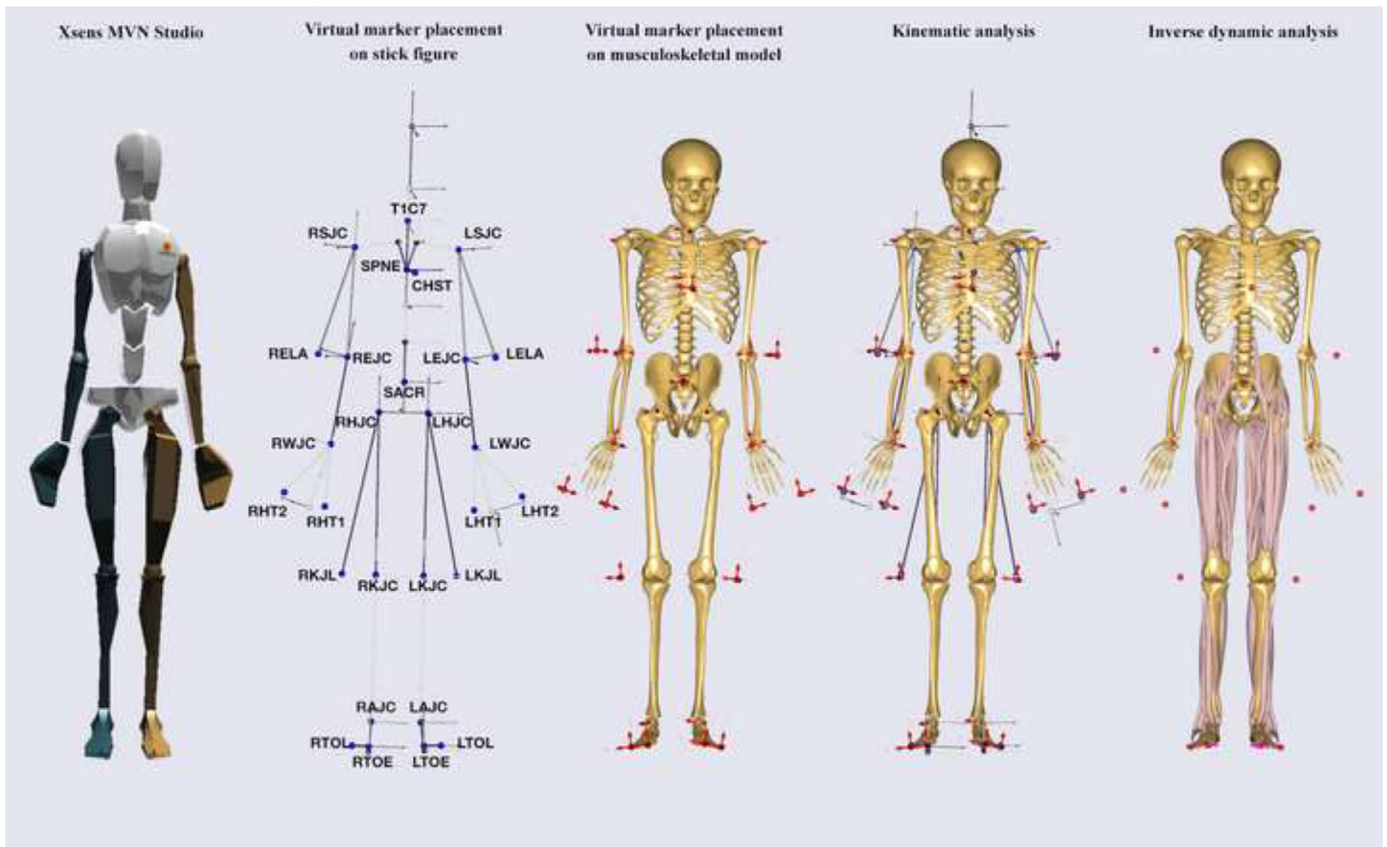


**Fig. 1.** Illustration of the pipeline used in the IMC-PGRF approach. A recording from Xsens MVN Studio (a) is exported to a BVH file to generate a stick figure model (b), in which virtual markers (blue) are placed. Virtual markers (red) are also placed on points of the musculoskeletal model (c), and by projecting b on c the kinematics of the musculoskeletal model are solved. Finally, inverse dynamic analysis using prediction of ground reaction forces and moments is performed to estimate the kinetics.

VMs are mapped to particular points of each model that are well defined in both models, such as joint centers and segment end points. The VM placement is illustrated in Fig. 1 and described in more detail in the supplementary material. Following this step, the VMs are treated as actual experimental markers, as if they were derived from an OMC system and they are assigned weights in three directions in the segmentframe. Contrary to OMC, no filtering was applied to the VM trajectories.

In all models, the GaitFullBody template of the AnyBody™ Managed Model Repository (AMMR) 1.6.2 was used to reconstruct the musculoskeletal models in AMS. The lumbar spine model was derived from the study of de Zee et al. [32], the lower limb model was derived from the Twente Lower Extremity Model Klein-Horsman et al. [33], and the shoulder and upper limb models were based on the model of the Delft Shoulder Group [34–36]. The full-body kinematic model contained 39 DOF in total. Specifically, a pelvis segment with three rotational and three translational DOF, two spherical hip joints, two revolute knee joints, two universal ankle joints, a spherical pelvic-lumbar joint, two glenohumeral joints with five DOF each, two universal elbow joints, and two universal wrist joints. The motion of the neck joint was locked to a neutral position.

### 2.5. Scaling and kinematics analysis of the musculoskeletal models

For each subject, a standing reference trial with an anatomical pose was utilized to identify the parameters of segment lengths and the (virtual) marker positions, using a least-square minimization between the model and input (virtual or skin-mounted) marker positions [37]. In the IMC-PGRF musculoskeletal model, the lengths of the shanks, thighs, head, upper arm and forearms were

derived directly from the stick figure, as generated from Xsens MVN studio using the measured body dimensions. In contrast, the pelvis width, foot length, and trunk height were optimized based on the above-mentioned least-square minimization method. The estimated segment lengths were used in all subsequent dynamic trials to perform the kinematic analysis based on the method of Andersen et al. [38].

### 2.6. Inertial and geometric scaling of the musculoskeletal models

The mass of each segment was linearly scaled based on the total body mass and the segment mass ratio values reported by Winter [4]. The inertial parameters were calculated by considering the segments as cylinders with uniform density. In addition, geometric scaling of each segment, where the longitudinal axis was defined as the second entry, was achieved using the following matrix:

$$S = \begin{bmatrix} \sqrt{\frac{m_s}{l_s}} & 0 & 0 \\ 0 & l_s & 0 \\ 0 & 0 & \sqrt{\frac{m_s}{l_s}} \end{bmatrix} \quad (1)$$

where  $S$  is the scaling matrix,  $l_s$  is the ratio between the unscaled and scaled lengths of the segment,  $m_s$  is the mass ratio of the segment.

### 2.7. Muscle recruitment

The muscle recruitment problem was solved by defining an optimization problem where a system of equations minimizes the cost function, subject to the dynamic equilibrium equations and

non-negativity constraints, so that each muscle can only pull, but not push, while its force remains below its strength [1,31,39].

The strengths of the muscles were derived from previous studies which described the models of the body parts, and were considered constant for different lengths and contraction velocities [32–36]. To scale the muscle strengths, fat percentage was used as in Veeger et al. [35], calculated from the body mass index [40]. The model of the lower body contained 110 muscles, distributed into 318 individual muscle paths. In contrast, in the upper body model, ideal joint torque generators were utilized. Actuators for residual forces and moments with capacity up to 10 N and Nm, respectively, were placed at the origin of the pelvis and included in the muscle recruitment problem previously described.

2.8. Ground reaction force and moment prediction

The GRF&M were predicted by adjusting a method of Skals et al. [23]. A set of eighteen dynamic contact points were overlaid 1 mm beneath the inferior surface of each foot. Each dynamic contact point consisted of five unilateral force actuators, which could generate a positive vertical force perpendicular to the ground, and static friction forces in the anterior, posterior, medial, and lateral directions using a friction coefficient of 0.5. In addition, the height and velocity activation thresholds were set to 0.03 m and 1.2 m/s, respectively.

2.9. Data analysis

Lower limb joint angles calculated in the IMC-PGRF model were compared to the OMC-PGRF/OMC-MGRF. In addition, GRF&M and JRF&M of the IMC-PGRF and OMC-PGRF were compared to OMC-MGRF.

Forces were normalized to body weight (BW) and moments to body weight times body height (BW\*BH). The time axis of the curves was normalized to 100% of the gait cycle for the kinematics (time between two consecutive heel-strike events of the analyzed limb) and 100% of the stance phase (time between heel-strike and toe-off events of the analyzed limb) for the kinetics. Measured and estimated GRF&M were expressed on the right handed coordinate frame defined by the walking direction within the trial (given that the subjects walked straight) and the vertical axis equal to the vertical axis of the respective motion capture system used. On the other hand, JRF&M were expressed on the coordinate frame of the segment distal to the body in both IMC and OMC methods.

The above-mentioned comparisons of kinematic and kinetic variables to their respective references were performed using absolute and relative root-mean-square-differences (RMSD and rRMSD, respectively) as described by Ren et al. [19]. In addition, for every curve, the magnitude (M) and phase (P) difference metrics [41] have been utilized. Pearson correlation coefficient (ρ) were calculated, averaged using Fisher’s z transformation method [42], and categorized similarly to Taylor [43], as “weak” (ρ ≤ 0.35),

“moderate” (0.35 < ρ ≤ 0.67), “strong” (0.67 < ρ ≤ 0.90), and “excellent” (ρ > 0.90).

3. Results

3.1. Estimated kinematics of the musculoskeletal model

Table 1 presents the results for the accuracy analysis for the joint angles of the IMC-driven model versus the OMC-driven model. Similarly, Fig. 2 illustrates the curves for the joint angles of the lower extremities averaged across all gait cycles performed by the eleven subjects. Excellent Pearson correlation coefficients have been found in all sagittal plane angles for ankle, knee, and hip (0.95, 0.99, and 0.99, respectively). For the same variables, the RMSDs across a gait cycle were found as 4.1 ± 1.3°, 4.4 ± 2.0° and 5.7 ± 2.1°, respectively (mean ± standard deviation). Hip flexion angles were overall underestimated (M = -4.0 ± 13.9%), whereas knee and ankle magnitude differences showed an average overestimation (0.7 ± 6.2% and 8.6 ± 16.4%). The hip abduction showed excellent correlations (ρ = 0.91) with an RMSD of 4.1 ± 2.0° and a mean underestimation with a magnitude difference M = -12.2 ± 34.7%. Strong correlation values (ρ = 0.68) were observed in the hip internal-external rotation angle with an RMSD of 6.5 ± 2.8° and an underestimation of magnitude difference M = 5.5 ± 39.0%. Finally, the subtalar eversion angle showed strong correlation (ρ = 0.82), RMSD of 9.66 ± 3.07° and M = 24.0 ± 34.7%.

3.2. Predicted kinetics using inertial and optical motion capture

The results of the accuracy analysis for GRF&M and JRF&M are presented in Tables 2 and 3, for IMC-PGRF and OMC-PGRF, respectively. The mean values and standard deviations of the curves from IMC-PGRF, OMC-PGRF, and OMC-MGRF models, are illustrated in Figs. 3 and 4, for the forces and moments, respectively.

The Pearson correlation coefficients of the IMC-PGRF model were excellent for vertical (ρ = 0.97) and anteroposterior GRF&M (ρ = 0.91) and strong for mediolateral GRF&M (ρ = 0.80). For the same components, RMSD values observed were of 9.3 ± 3.0, 5.5 ± 1.2 and 2.1 ± 0.6 %BW, respectively (mean ± standard deviation). The OMC-PGRF model performed better in the anteroposterior GRF&M components (ρ = 0.96, RMSD = 3.7 ± 1.1 %BW), and similarly to IMC-PGRF for the other two GRF&M components (mediolateral: ρ = 0.79, RMSD = 1.9 ± 0.5 BW, vertical: ρ = 0.99, RMSD = 5.9 ± 1.9 BW).

Concerning GRM, the sagittal plane was predicted with similar excellent correlations in both IMC-PGRF (ρ = 0.91) and OMC-PGRF (ρ = 0.94) driven models. The correlation coefficients for frontal and transverse GRM components found in the IMC-PGRF model were ρ = 0.64, ρ = 0.82, respectively, whereas in the OMC-PGRF model (ρ = 0.66, ρ = 0.81, respectively). The RMSDs found in the IMC-PGRF approach were 0.9 ± 0.6, 1.6 ± 0.6, and 0.2 ± 0.001 %BW\*BH for frontal, sagittal and transverse GR&M, respectively,

**Table 1**  
Comparison of lower limb joint angles between musculoskeletal model driven by the inertial (IMC-PGRF) and optical motion capture (OMC-PGRF/OMC-MGRF), using Pearson correlation coefficient (ρ), absolute and relative root-mean-squared-differences (RMSD and rRMSD in %, respectively). M and P denote the % magnitude and phase differences.

	ρ	RMSD	rRMSD	M	P
Subtalar eversion	0.81	9.7 (3.2)	32.6 (10.3)	24.0 (34.7)	19.3 (10.2)
Ankle plantarflexion	0.95	4.1 (1.3)	14.0 (4.8)	8.6 (16.4)	9.8 (3.9)
Knee flexion	0.99	4.4 (2.0)	7.2 (3.4)	0.7 (6.2)	4.8 (2.7)
Hip abduction	0.91	4.1 (2.0)	25.9 (10.7)	-12.2 (34.7)	21.2 (9.3)
Hip external rotation	0.68	6.5 (2.8)	36.9 (15.2)	5.5 (39.0)	12.6 (6.2)
Hip flexion	0.99	5.7 (2.1)	12.7 (5.3)	-4.0 (13.9)	8.8 (4.2)

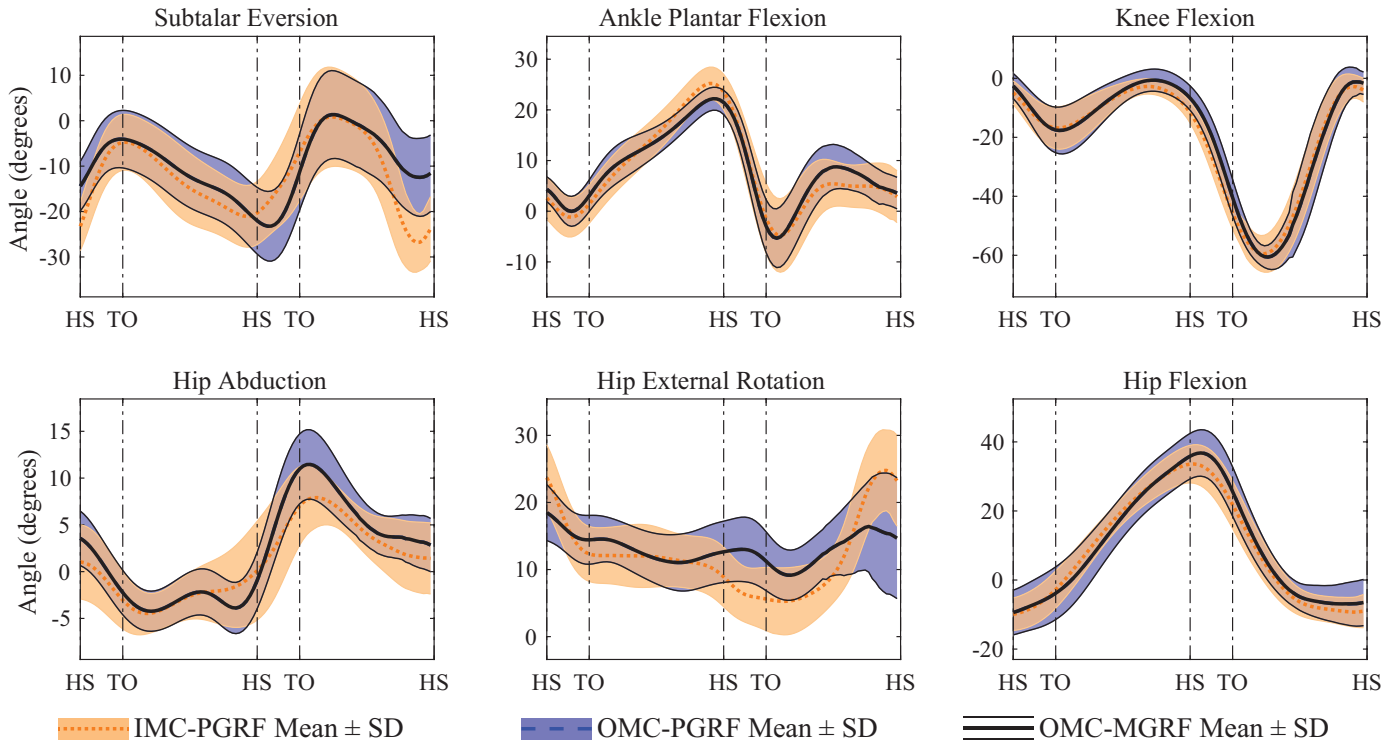


Fig. 2. Ankle, knee, and hip joint angle estimates (standard deviation around mean) of the IMC-PGRF (orange shaded area around orange dotted line) and OMC-PGRF models (blue shaded area around blue dashed line) versus OMC-MGRF model (thin black solid lines around thick black solid line).

Table 2

IMC-PGRF-based ground and joint reaction forces (first three quantities) and net moments (second three quantities) versus OMC-MGRF. Pearson correlation coefficient is denoted with  $\rho$ . Absolute per body weight (or body weight times height) and relative root-mean-squared-difference are denoted with  $RMSD$  (%BW or %BW $\cdot$ BH) and  $rRMSD$  (%), respectively.  $M$  and  $P$  indicate the magnitude and phase differences (%).

	$\rho$	$RMSD$	$rRMSD$	$M$	$P$
<b>Ground</b>					
Anteroposterior	0.91	5.5 (1.2)	15.0 (2.4)	-25.4 (7.3)	14.4 (3.2)
Mediolateral	0.80	2.1 (0.6)	18.5 (3.2)	7.3 (19.3)	15.4 (3.8)
Vertical	0.97	9.3 (3.0)	7.7 (2.1)	-1.5 (1.5)	3.4 (1.0)
Frontal	0.64	0.9 (0.6)	38.0 (23.1)	125.5 (319.9)	30.6 (17.3)
Sagittal	0.91	1.6 (0.6)	17.5 (6.8)	14.3 (18.2)	12.1 (4.5)
Transverse	0.82	0.2 (0.1)	23.3 (7.2)	-8.5 (41.9)	17.8 (5.3)
<b>Ankle</b>					
Anteroposterior	0.84	22.2 (10.3)	26.1 (10.2)	49.0 (45.8)	10.8 (2.1)
Mediolateral	0.93	24.3 (8.9)	15.2 (5.3)	14.3 (17.1)	7.9 (2.7)
Proximodistal	0.93	88.5 (30.6)	13.6 (4.6)	9.8 (14.1)	7.2 (2.3)
Eversion	0.76	0.6 (0.2)	33.3 (20.2)	107.7 (220.3)	18.9 (10.7)
Plantar flexion	0.93	1.6 (0.6)	15.1 (6.6)	10.6 (18.1)	9.9 (3.6)
Axial	0.67	0.5 (0.2)	30.4 (12.2)	46.5 (49.1)	27.2 (13.5)
<b>Knee</b>					
Anteroposterior	0.82	30.6 (10.3)	25.8 (9.7)	43.7 (53.5)	13.0 (4.5)
Mediolateral	0.91	12.0 (3.5)	14.1 (3.8)	6.6 (8.6)	7.0 (2.0)
Proximodistal	0.90	63.1 (26.9)	14.3 (6.6)	5.1 (9.1)	7.2 (2.8)
Abduction	0.81	1.1 (0.4)	18.9 (6.8)	-2.7 (16.1)	10.7 (3.8)
Flexion	0.58	1.9 (0.5)	29.8 (7.6)	17.9 (45.0)	32.8 (9.6)
Axial	0.73	0.3 (0.1)	25.4 (10.3)	2.3 (30.5)	27.9 (13.8)
<b>Hip</b>					
Anteroposterior	0.71	17.6 (7.6)	27.2 (9.6)	6.8 (24.4)	27.6 (10.9)
Mediolateral	0.73	27.0 (12.5)	23.0 (7.4)	7.7 (14.6)	10.6 (4.1)
Proximodistal	0.78	102.8 (30.6)	21.7 (4.5)	20.2 (10.0)	9.0 (2.5)
Abduction	0.83	1.4 (0.7)	19.7 (5.8)	6.3 (16.9)	13.7 (7.9)
Flexion	0.92	2.2 (0.6)	19.4 (4.2)	73.2 (26.3)	14.8 (4.2)
External rotation	0.50	0.5 (0.2)	31.6 (6.6)	-3.9 (36.4)	25.6 (10.1)

**Table 3**

OMC-PGRF-based ground and joint reaction forces (first three quantities) and net moments (second three quantities) versus OMC-MGRF. Pearson correlation coefficient is denoted with  $\rho$ . Absolute per body weight (or body weight times height) and relative root-mean-squared-difference are denoted with RMSD (%BW or %BW\*BH) and rRMSD (%), respectively.  $M$  and  $P$  indicate the magnitude and phase differences (%).

	$\rho$	RMSD	rRMSD	M	P
<b>Ground</b>					
Anteroposterior	0.96	3.7 (1.1)	8.3 (2.0)	7.7 (12.0)	8.8 (1.8)
Mediolateral	0.79	1.9 (0.5)	18.6 (4.1)	2.4 (10.8)	15.2 (4.9)
Vertical	0.99	5.9 (1.9)	4.9 (1.4)	-1.2 (1.1)	2.1 (0.7)
Frontal	0.66	0.7 (0.2)	30.3 (9.3)	71.0 (122.2)	24.5 (9.1)
Sagittal	0.94	1.2 (0.4)	13.1 (3.8)	15.9 (15.3)	9.2 (3.2)
Transverse	0.81	0.2 (0.1)	20.7 (7.5)	7.1 (22.9)	17.5 (7.5)
<b>Ankle</b>					
Anteroposterior	0.83	18.9 (6.9)	23.0 (6.1)	37.3 (28.6)	10.8 (2.3)
Mediolateral	0.96	16.1 (4.2)	10.7 (2.6)	6.8 (9.6)	5.8 (2.1)
Proximodistal	0.96	62.2 (17.6)	9.8 (2.7)	7.1 (9.0)	5.2 (1.8)
Eversion	0.76	0.5 (0.1)	25.5 (7.0)	45.3 (64.1)	18.7 (10.2)
Plantar flexion	0.96	1.0 (0.3)	10.1 (3.3)	5.9 (10.0)	7.0 (2.6)
Axial	0.64	0.5 (0.1)	27.2 (7.3)	33.3 (36.9)	27.5 (11.5)
<b>Knee</b>					
Anteroposterior	0.93	11.9 (4.5)	12.3 (4.3)	-7.3 (8.7)	7.4 (2.0)
Mediolateral	0.96	7.2 (2.0)	8.8 (2.6)	-4.2 (5.6)	4.4 (1.0)
Proximodistal	0.95	41.7 (12.0)	9.3 (2.6)	-2.7 (5.8)	4.9 (1.2)
Abduction	0.91	0.8 (0.2)	12.6 (2.6)	-0.1 (10.5)	7.7 (1.6)
Flexion	0.86	0.9 (0.3)	16.7 (4.8)	-1.7 (14.3)	16.9 (5.2)
Axial	0.82	0.2 (0.1)	18.5 (6.6)	-3.4 (17.7)	20.6 (8.0)
<b>Hip</b>					
Anteroposterior	0.89	9.9 (3.6)	16.0 (6.7)	-10.4 (10.6)	16.6 (7.6)
Mediolateral	0.92	14.7 (4.0)	12.7 (3.1)	-1.9 (6.9)	6.2 (1.5)
Proximodistal	0.92	50.0 (15.9)	11.5 (2.6)	-4.6 (6.1)	5.5 (1.2)
Abduction	0.91	0.8 (0.2)	13.3 (2.6)	-3.2 (6.3)	8.7 (2.4)
Flexion	0.86	1.3 (0.4)	16.4 (3.4)	-9.3 (12.3)	18.0 (4.1)
External rotation	0.68	0.3 (0.1)	22.5 (3.7)	6.5 (15.8)	18.8 (4.8)

which were either slightly higher or similar to the RMSDs of the OMC-PGRF approach ( $0.7 \pm 0.2$ ,  $1.2 \pm 0.4$ , and  $0.2 \pm 0.1$  %BW\*BH, respectively).

#### 4. Discussion

We have presented a method to perform musculoskeletal model-based inverse dynamics using exclusively IMC input (IMC-PGRF). First, we compared the kinematic joint angle estimates of the lower limbs against those assessed through a conventional, laboratory-based OMC input. In addition, we tested the performance of the approach in calculating the JRF&M, while predicting the GRF&M from the kinematics, against a similarly constructed model (OMC-MGRF) which uses input from both FP and OMC. Finally, we performed a similar comparison to evaluate the predicted kinetics of a model driven exclusively by OMC input (OMC-PGRF).

Regarding the IMC-based joint angles in the musculoskeletal model, all three sagittal plane angles provided excellent correlations (range: 0.95–0.99) and average RMSD values remained below 6°. Slightly lower correlations were observed in the frontal and transverse plane angles, which can be explained due to the smaller range of motion within these planes. For instance, even though the hip abduction and external rotation joint angles present absolute RMSD values similar to the flexion component, their rRMSDs which take into account the range of motion are two and three times higher, respectively.

Both GRF&M and JRF&M of the vertical axis presented higher correlations and lower RMSDs than the ones in the anteroposterior and mediolateral axes. Similarly, sagittal plane moments were found in most cases to be more accurate than frontal and transverse plane moments. By visual inspection of the curves, we ob-

serve that the magnitude of the IMC-PGRF anteroposterior GRF&M seems to be underestimated both in the negative early stance and positive late stance peak, which can be confirmed by the magnitude difference for that curve ( $M = -28.3\%$ ). However, this behavior is not observed in the OMC-PGRF, nor during the single stance of the IMC-PGRF curve. Despite the higher rRMSD found in the non-sagittal joint angles, the performance of the IMC-PGRF in the mediolateral, frontal and transverse plane GRF&M components matched closely the OMC-PGRF approach. This observation reveals that OMC-based kinematics suffer from errors of similar size, when capturing the typically small movements of the frontal and transverse planes, given the fact that both IMC-PGRF and OMC-PGRF had the same model characteristics. Therefore, OMC-MGRF should also be used with caution, when comparing either kinematic or JRF&M quantities of the non-sagittal planes.

A number of error sources contribute to discrepancies in the OMC kinematics. First, soft tissue artifacts can create a relative movement of the marker with respect to the bone [44,45]. In addition, mismatches between the experimental and modeled marker positions can lead to errors in segment orientations calculated during inverse kinematics. Both error sources would have a relatively larger impact on the kinematics of the frontal and transverse plane, than on the sagittal plane. Finally, the JRF&M of the OMC-PGRF were compared against a non-independent OMC-MGRF reference, which could have contributed to underestimation of the actual errors.

The IMC-PGRF approach has a number of possible sources of errors which would influence the performance. Similarly to OMC models, soft-tissue artifacts may compromise the kinematic estimates. Further errors in segment kinematics may stem due to the N-pose calibration assumptions. In particular, mismatches between the practised and modeled N-pose could result in offsets in the

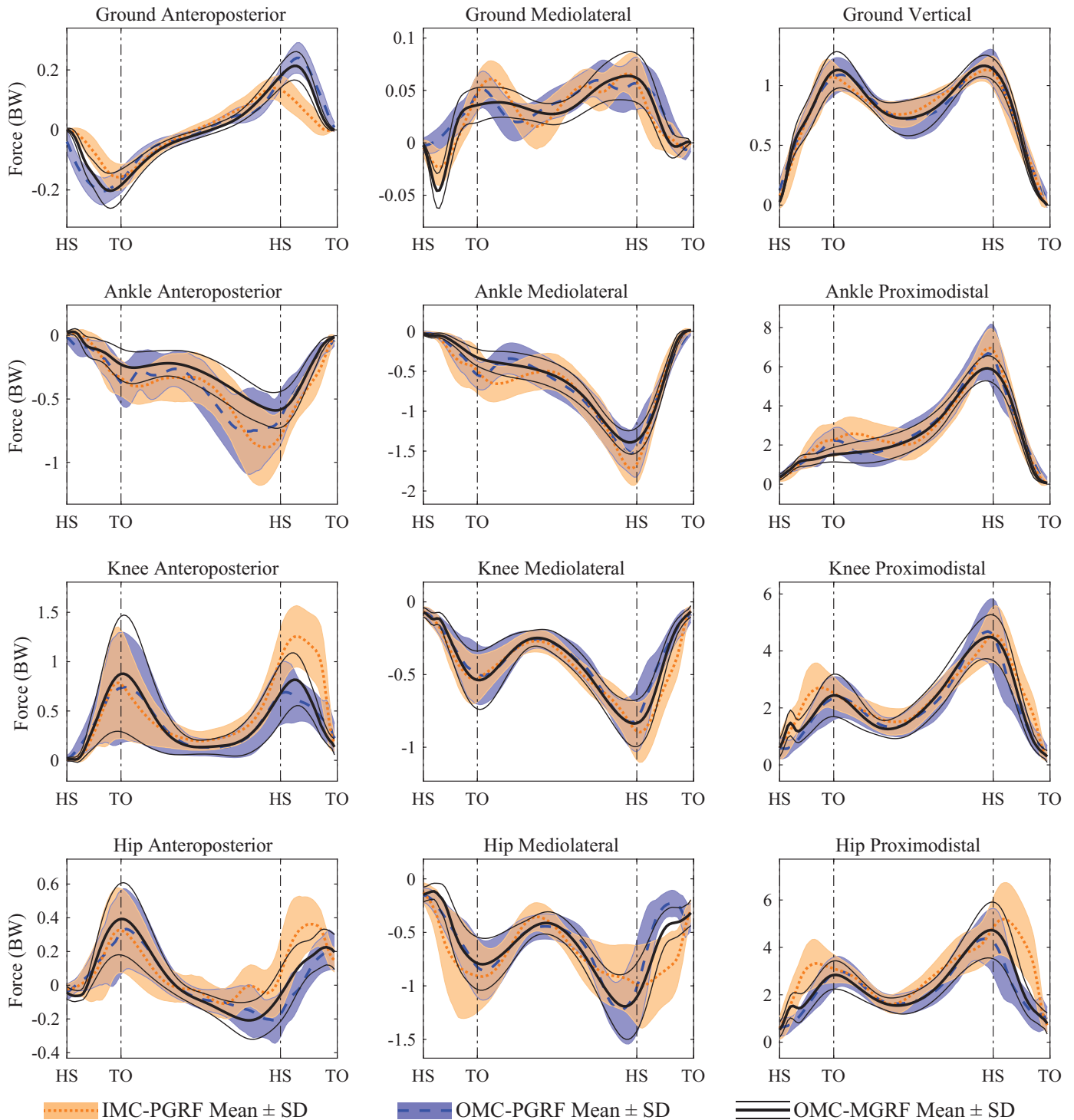


**Fig. 3.** Ground and lower limb joint reaction force estimates (standard deviation around mean) of the IMC-PGRF (orange shaded area around orange dotted line) and OMC-PGRF models (blue shaded area around blue dashed line) versus OMC-MGRF model (thin black solid lines around thick black solid line).

estimated positions. Other common error sources in IMC include manual measurements of segment lengths as well as IMU inaccuracies. In addition, the stick figure model, which was utilized to recreate the VMs, has a higher number of DOF, compared to the musculoskeletal model used.

A possible source of error in all inverse dynamic approaches concerns the inertial parameters (masses and moments of inertia), as well as the center of mass (CoM) locations of each human body

segment, which were calculated based on anthropometric tables found in the literature.

This study focused on presenting and evaluating a general workflow for musculoskeletal model-based inverse dynamic simulations using ambulatory IMC systems. The presentation of results in this study was performed on the level of ground and joint reaction forces and moments. These measures are calculated from muscle force estimates derived from a muscle

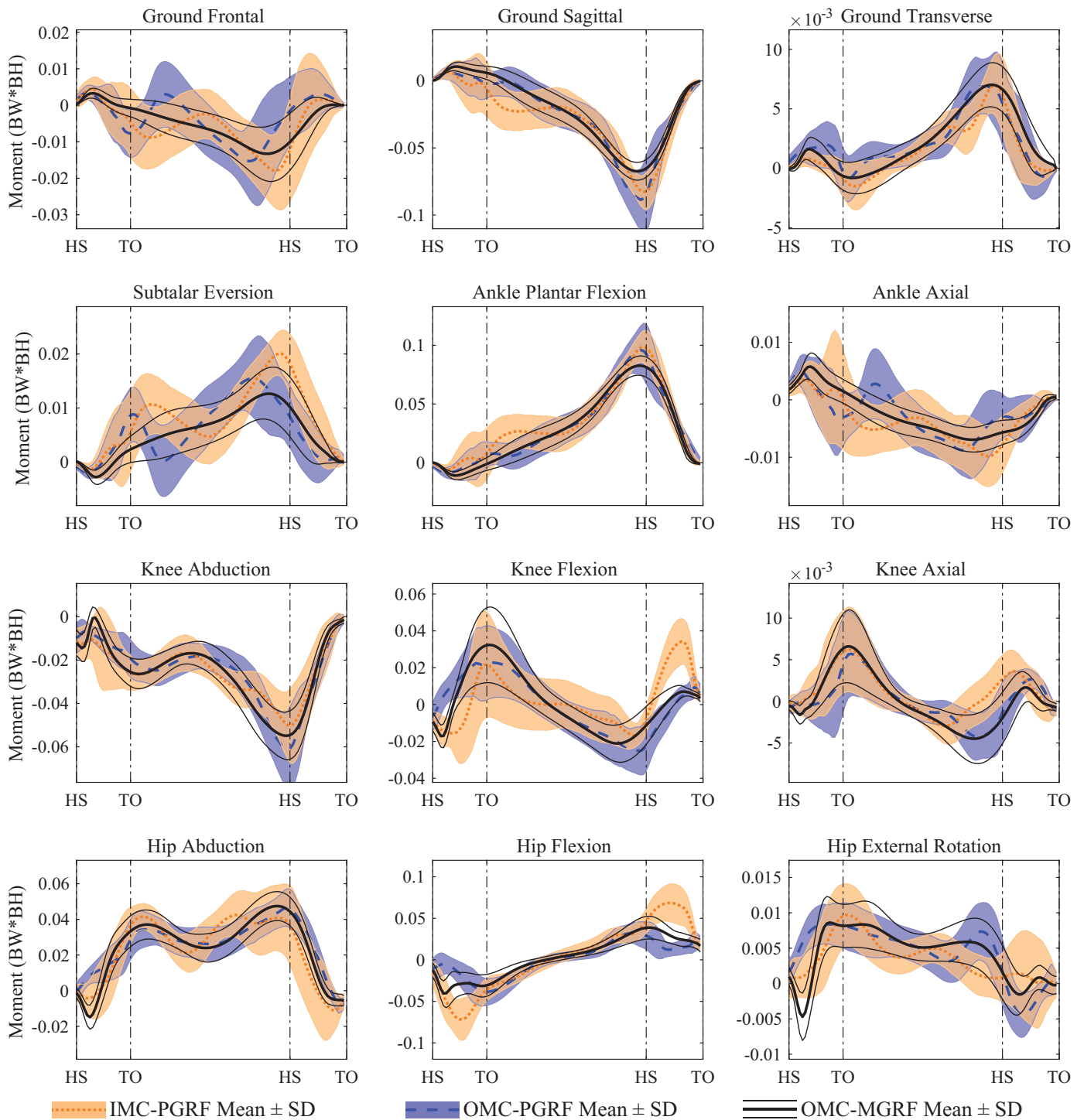


**Fig. 4.** Ground reaction and lower limb net joint moment estimates (standard deviation around mean) of the IMC-PGRF (orange shaded area around orange dotted line) and OMC-PGRF models (blue shaded area around blue dashed line) versus OMC-MGRF model (thin black solid lines around thick black solid line).

recruitment optimization technique. Given the high number of muscles in the model (110) and without a clear medical research question, it is challenging to choose which muscles are more important to present and analyze. Future studies could examine specific applications and pathologies in order to identify the most important muscles and evaluate their respective force estimates.

A limitation of this study is that, even though the method has been previously shown to be universally applicable in OMC-

based studies [22,23], we only evaluated its performance in gait of three different speeds. In addition, our experiments included only young healthy male subjects, but the underlying methods to predict kinetics from kinematics have been recently shown to be applicable in Parkinson’s patients [46]. Future studies could investigate the application of IMC systems combined with musculoskeletal modeling in groups of larger sample size than the current study, including patients, as well as female subjects.

## 5. Conclusion

In this study, we have demonstrated a workflow to perform musculoskeletal model-based inverse dynamics using input from a commercially available IMC system. Our validation findings indicate that the prediction of GRF&M as well as JRF&M using musculoskeletal model-based inverse dynamics based on only IMC data provides comparable performance to both OMC-PGRF and OMC-MGRF methods. The proposed method allows assessment of kinetic variables outside the laboratory.

## Ethical approval

The ethical guidelines of The Scientific Ethical Committee for the Region of North Jutland (Den Videnskabetiske Komit for Region Nordjylland) were followed and all volunteers signed written informed consent after receiving detailed information prior to data collection.

## Conflict of interest

Three of the authors are employees of Xsens Technologies B.V. that manufactures and sells the Xsens MVN. One of the authors is employee of AnyBody Technology A/S that owns and sells the AnyBody Modeling System.

## Acknowledgments

This study was performed in the context of KNEEMO Initial Training Network, funded by the [European Union's Seventh Framework Programme](#) for research, technological development, and demonstration under Grant Agreement No. 607510 ([www.kneemo.eu](http://www.kneemo.eu)). This work was also supported by the Danish Council for Independent Research under grant no. DFF-4184-00018 to M. S. Andersen. Finally, this research received funding in part from the [European Union's Horizon 2020](#) research and innovation programme under grant agreement No. 680754 (The MovAiD project, [www.movaid.eu](http://www.movaid.eu)).

## References

- [1] Damsgaard M, Rasmussen J, Christensen ST, Surma E, de Zee M. Analysis of musculoskeletal systems in the anybody modeling system. *Simul Model Pract Theory* 2006;14(8):1100–11.
- [2] Delp SL, Anderson FC, Arnold AS, Loan P, Habib A, John CT, et al. OpenSim: open-source software to create and analyze dynamic simulations of movement. *IEEE Trans Biomed Eng* 2007;54(11):1940–50. doi:10.1109/TBME.2007.901024.
- [3] Erdemir A, McLean S, Herzog W, van den Bogert AJ. Model-based estimation of muscle forces exerted during movements. *Clin Biomech* 2007;22(2):131–54. doi:10.1016/j.clinbiomech.2006.09.005.
- [4] Winter DA. *Biomechanics and Motor Control of Human Movement*. New York: Wiley; 1990.
- [5] Rasmussen J, Damsgaard M, Voigt M. Muscle recruitment by the min/max criterion – a comparative numerical study. *J Biomech* 2001;34(3):409–15. doi:10.1016/S0021-9290(00)00191-3.
- [6] Challis JH. The variability in running gait caused by force plate targeting. *J Appl Biomech* 2001;17(1):77–83.
- [7] Riemer R, Hsiao-Weckler ET, Zhang X. Uncertainties in inverse dynamics solutions: a comprehensive analysis and an application to gait. *Gait Posture* 2008;27(4):578–88. doi:10.1016/j.gaitpost.2007.07.012.
- [8] Hatze H. The fundamental problem of myoskeletal inverse dynamics and its implications. *J Biomech* 2002;35(1):109–15. doi:10.1016/S0021-9290(01)00158-0.
- [9] Veltink PH, Liedtke C, Droog E, Van Der Kooij H. Ambulatory measurement of ground reaction forces. *IEEE Trans Neural Syst Rehabil Eng* 2005;13(3):423–7. doi:10.1109/TNSRE.2005.847359.
- [10] Schepers HM, Koopman HFJM, Veltink PH. Ambulatory assessment of ankle and foot dynamics. *IEEE Trans Biomed Eng* 2007;54(5):895–902. doi:10.1109/TBME.2006.889769.
- [11] Liu T, Inoue Y, Shibata K. A wearable force plate system for the continuous measurement of triaxial ground reaction force in biomechanical applications. *Meas Sci Technol* 2010;21(8). doi:10.1088/0957-0233/21/8/085804.
- [12] Former Cordero A, Koopman HFJM, Van Der Helm FCT. Use of pressure insoles to calculate the complete ground reaction forces. *J Biomech* 2004;37(9):1427–32. doi:10.1016/j.jbiomech.2003.12.016.
- [13] Rouhani H, Favre J, Crevoisier X, Aminian K. Ambulatory assessment of 3D ground reaction force using plantar pressure distribution. *Gait Posture* 2010;32(3):311–16. doi:10.1016/j.gaitpost.2010.05.014.
- [14] Jung Y, Jung M, Lee K, Koo S. Ground reaction force estimation using an insole-type pressure mat and joint kinematics during walking. *J Biomech* 2014;47(11):2693–9. doi:10.1016/j.jbiomech.2014.05.007.
- [15] Van Den Noort J, Van Der Esch M, Steultjens MP, Dekker J, Schepers HM, Veltink PH, et al. Influence of the instrumented force shoe on gait pattern in patients with osteoarthritis of the knee. *Med Biol Eng Comput* 2011;49(12):1381–92. doi:10.1007/s11517-011-0818-z.
- [16] Liedtke C, Fokkenrood SAW, Menger JT, van der Kooij H, Veltink PH. Evaluation of instrumented shoes for ambulatory assessment of ground reaction forces. *Gait Posture* 2007;26(1):39–47. doi:10.1016/j.gaitpost.2006.07.017.
- [17] Low DC, Dixon SJ. Footscan pressure insoles: accuracy and reliability of force and pressure measurements in running. *Gait Posture* 2010;32(4):664–6. doi:10.1016/j.gaitpost.2010.08.002.
- [18] Audu ML, Kirsch RF, Triolo RJ. Experimental verification of a computational technique for determining ground reactions in human bipedal stance. *J Biomech* 2007;40(5):1115–24. doi:10.1016/j.jbiomech.2006.04.016.
- [19] Ren L, Jones RK, Howard D. Whole body inverse dynamics over a complete gait cycle based only on measured kinematics. *J Biomech* 2008;41(12):2750–9. doi:10.1016/j.jbiomech.2008.06.001.
- [20] Oh SE, Choi A, Mun JH. Prediction of ground reaction forces during gait based on kinematics and a neural network model. *J Biomech* 2013;46(14):2372–80. doi:10.1016/j.jbiomech.2013.07.036.
- [21] Choi A, Lee J-M, Mun JH. Ground reaction forces predicted by using artificial neural network during asymmetric movements. *Int J Precis Eng Manuf* 2013;14(3):475–83. doi:10.1007/s12541-013-0064-4.
- [22] Fluit R, Andersen MS, Kolk S, Verdonshot N, Koopman HFJM. Prediction of ground reaction forces and moments during various activities of daily living. *J Biomech* 2014;47(10):2321–9. doi:10.1016/j.jbiomech.2014.04.030.
- [23] Skals S, Jung M, Damsgaard M, Andersen MS. Prediction of ground reactions forces and moments during sports-related movements. *Multibody Syst Dyn* 2016;39(3):175–95.
- [24] Luinge HJ, Veltink PH. Measuring orientation of human body segments using miniature gyroscopes and accelerometers. *Med Biol Eng Comput* 2005;43(2):273–82. doi:10.1007/BF02345966.
- [25] Roetenberg D, Luinge HJ, Baten CTM, Veltink PH. Compensation of magnetic disturbances improves inertial and magnetic sensing of human body segment orientation. *IEEE Trans Neural Syst Rehabil Eng* 2005;13(3):395–405. doi:10.1109/TNSRE.2005.847353.
- [26] Roetenberg D, Luinge HJ, Slycke P. Xsens MVN: Full 6DOF human motion tracking using miniature inertial sensors (Technical report). Xsens Technologies B.V. Enschede; 2013. <http://www.xsens.com>.
- [27] Zhang J-T, Novak AC, Brouwer B, Li Q. Concurrent validation of Xsens MVN measurement of lower limb joint angular kinematics. *Physiol Meas* 2013;34(8):N63–9. doi:10.1088/0967-3334/34/8/N63.
- [28] Karatsidis A, Bellusci G, Schepers HM, de Zee M, Andersen MS, Veltink PH. Estimation of ground reaction forces and moments during gait using only inertial motion capture. *Sensors (Switzerland)* 2017;17(1). doi:10.3390/s17010075.
- [29] Koning BHW, van der Krogt MM, Baten CTM, Koopman BFJM. Driving a musculoskeletal model with inertial and magnetic measurement units. *Comput Methods Biomech Biomed Eng* 2015;18(9):1003–13. doi:10.1080/10255842.2013.867481.
- [30] Xsens MVN Studio User Manual. Revision T. March 2017 [Accessed 31 January 2019] [http://issuu.com/xsensmvn/docs/mvn\\_user\\_manual\\_71c37181653db5](http://issuu.com/xsensmvn/docs/mvn_user_manual_71c37181653db5).
- [31] Skals S, Rasmussen K, Bendtsen K, Yang J, Andersen M. A musculoskeletal model driven by dual microsoft Kinect sensor data. *Multibody System Dynamics* 2017. doi:10.1007/s11044-017-9573-8.
- [32] de Zee M, Hansen L, Wong C, Rasmussen J, Simonsen EB. A generic detailed rigid-body lumbar spine model. *J Biomech* 2007;40(6):1219–27. doi:10.1016/j.jbiomech.2006.05.030.
- [33] Klein Horsman MD, Koopman HFJM, van der Helm FCT, Pros LP, Veeger HEJ. Morphological muscle and joint parameters for musculoskeletal modelling of the lower extremity. *Clin Biomech* 2007;22(2):239–47. doi:10.1016/j.clinbiomech.2006.10.003.
- [34] Veeger HEJ, Van Der Helm FCT, Van Der Woude LHV, Pronk GM, Rozendal RH. Inertia and muscle contraction parameters for musculoskeletal modelling of the shoulder mechanism. *J Biomech* 1991;24(7):615–29. doi:10.1016/0021-9290(91)90294-W.
- [35] Veeger HEJ, Yu B, An K-N, Rozendal RH. Parameters for modeling the upper extremity. *J Biomech* 1997;30(6):647–52. doi:10.1016/S0021-9290(97)00011-0.
- [36] Van der Helm FCT, Veeger HEJ, Pronk GM, Van der Woude LHV, Rozendal RH. Geometry parameters for musculoskeletal modelling of the shoulder system. *J Biomech* 1992;25(2):129–44. doi:10.1016/0021-9290(92)90270-B.
- [37] Andersen MS, Damsgaard M, MacWilliams B, Rasmussen J. A computationally efficient optimisation-based method for parameter identification of kinematically determinate and over-determinate biomechanical systems. *Comput Methods Biomech Biomed Eng* 2010;13(2):171–83. doi:10.1080/10255840903067080.

- [38] Andersen MS, Damsgaard M, Rasmussen J. Kinematic analysis of over-determinate biomechanical systems. *Comput Methods Biomech Biomed Eng* 2009;12(4):371–84. doi:[10.1080/10255840802459412](https://doi.org/10.1080/10255840802459412).
- [39] Marra MA, Vanheule V, Fluit R, Koopman BHFJM, Rasmussen J, Verdonchot N, et al. A subject-specific musculoskeletal modeling framework to predict in vivo mechanics of total knee arthroplasty. *J Biomech Eng* 2015;137(2). doi:[10.1115/1.4029258](https://doi.org/10.1115/1.4029258).
- [40] Frankenfield DC, Rowe WA, Cooney RN, Smith JS, Becker D. Limits of body mass index to detect obesity and predict body composition. *Nutrition* 2001;17(1):26–30. doi:[10.1016/S0899-9007\(00\)00471-8](https://doi.org/10.1016/S0899-9007(00)00471-8).
- [41] Sprague MA, Geers TL. Spectral elements and field separation for an acoustic fluid subject to cavitation. *J Comput Phys* 2003;184(1):149–62. doi:[10.1016/S0021-9991\(02\)00024-4](https://doi.org/10.1016/S0021-9991(02)00024-4).
- [42] Silver NC, Dunlap WP. Averaging correlation coefficients: should Fisher's z transformation be used? *J Appl Psychol* 1987;72(1):146.
- [43] Taylor R. Interpretation of the correlation coefficient: a basic review. *J Diagn Med Sonogr* 1990;6(1):35–9. doi:[10.1177/875647939000600106](https://doi.org/10.1177/875647939000600106).
- [44] Chiari L, Croce UD, Leardini A, Cappozzo A, Chiari L, Croce UD, et al. Human movement analysis using stereophotogrammetry. *Gait Posture* 2005;21:226–37.
- [45] Leardini A, Chiari A, Della Croce U, Cappozzo A. Human movement analysis using stereophotogrammetry part 3. Soft tissue artifact assessment and compensation. *Gait Posture* 2005;21(2):212–25. doi:[10.1016/j.gaitpost.2004.05.002](https://doi.org/10.1016/j.gaitpost.2004.05.002).
- [46] Eltoukhy M, Kuenze C, Andersen MS, Oh J, Signorile J. Prediction of ground reaction forces for Parkinson's disease patients using a Kinect-driven musculoskeletal gait analysis model. *Med Eng Phys* 2017;50:75–82. doi:[10.1016/j.medengphy.2017.10.004](https://doi.org/10.1016/j.medengphy.2017.10.004).